UDK 666.762.11:57.012.3
Original scientific article/Izvirni znanstveni članek

ISSN 1580-2949
Mater. Tehnol.

EFFECTS OF MANGANESE DIOXIDE AND SINTERING TEMPERATURE ON THE PROPERTIES AND MICROSTRUCTURE OF A SECONDARY-ALUMINUM-ASH CERAMIC PROPPANT

VPLIV DODATKA MANGANOVEGA DIOKSIDA IN TEMPERATURE SINTRANJA NA LASTNOSTI TER MIKROSTRUKTURO KERAMIČNEGA POLNILA NA OSNOVI PEPELA SEKUNDARNEGA ALUMINIJA

Yongming Zeng[1], Naichen Xiao[2], Haiping Yang[1], Peipeng Yang[1], Fei Yan[1], Sifeng Bi[1], Ruien Yu[1,2*]

[1]Xinjiang Key Laboratory of High Value Green Utilization of Low-Rank Coal, School of Chemistry and Chemical Engineering, Changji University, Changji 831100, China
[2]Shanxi Key Laboratory of Advanced Manufacturing Technology, School of Mechanical Engineering, North University of China, Taiyuan 030051, China

Prejem rokopisa – received: 2025-04-18; sprejem za objavo – accepted for publication: 2025-08-29

doi:10.17222/mit.2025.1442

In this study, a ceramic proppant for hydraulic fracturing in oil and gas extraction was prepared by sintering secondary aluminum ash as the main raw material, kaolin as the auxiliary material and manganese dioxide as the additive. The effects of different proportions of manganese dioxide on the physical phase composition and microscopic morphology of the proppant were analyzed with X-ray diffraction and scanning electron microscopy at sintering temperatures of 1170–1270 °C. The results showed that at 1270 °C, the crushing rate of the sample with a 2 *w*/% manganese dioxide addition was 8.41 %, and the main crystalline phase consisted of corundum and a small amount of mullite. With the addition of manganese dioxide, the ternary eutectic system of MnO_2-Al_2O_3-SiO_2 increases, which lowers the corundum generation temperature, accelerates its growth rate and improves the crushing resistance. This study solves the problem of weak crushing resistance of the ceramic-granule proppant prepared from secondary aluminum ash, and achieves an efficient use of waste, which is of great significance for environmental protection and resource recycling.

Keywords: ceramic proppant, secondary aluminum ash, crushing rate, microstructure

V članku avtorji opisujejo študijo priprave keramičnega propanta (polnila; angl.: proppant) za hidravlično lomljenje med pridobivanjem mineralnega olja in nafte. Propant so izdelali s sintranjem pepela (pretežno Al oksid), nastalega med predelavo sekundarnega aluminija, kateremu so dodali še kaolin in manganov dioksid. Sintranje so izvajali pri temperaturah med 1170 °C in 1270 °C. Nato so s pomočjo rentgenske difrakcije (XRD) in vrstičnega elektronskega mikroskopa (SEM) študirali vpliv različnega deleža dodanega MnO_2 na fizikalno-kemijsko fazno stavo in mikroskopsko morfologijo nastalega sintranega materiala. Rezultati analiz so pokazali, da je bila stopnja drobljenja sintranega materiala 8,41%-na po sintranju na temperaturi 1270 °C in 2 *w*/% dodatka MnO_2. Njegova glavna kristalinična faza je bila korund in preostanek majhen delež mulita. Z naraščanjem dodatka MnO_2 se v ternarnem evtektskem sistemu MnO_2-Al_2O_3-SiO_2 znižuje temperatura tvorbe korunda, pospešuje njegova hitrost rasti in zato izboljšuje odpornost proti drobljenju. S to študijo so avtorji rešili problem šibke odpornosti keramičnih granul opanta proti drobljenju, izdelanega iz pepela nastalega pri predelavi sekundarnega aluminija in dosegli učinkovito uporabo odpadnega materiala, kar je zelo pomembno za zaščito okolja in recikliranje odpadnih surovin.

Ključne besede: keramično polnilo (propant), pepel sekundarnega aluminija, hitrost drobljenja, mikrostruktura

1 INTRODUCTION

With the development of industrial economy, the importance of petroleum has become increasingly prominent. It plays an irreplaceable role in energy supply, chemical raw materials, national security, technological innovation and industrial upgrading. In this context hydraulic fracturing extraction technology came into being, as it is an important means to increase the production of oil and gas, effectively overcoming the challenges of developing low-permeability and ultra-deep oil and gas reservoirs.[1] Currently, hydraulic fracturing plays a crucial role in extracting oil from low-permeability oilfields. Fracturing proppant is an indispensable material in oil extraction activities,[2] transported into formations with low permeability and poor physical properties through the hydraulic fracturing fluid. It prevents fracture closure and increases fracture conductivity, having an excellent effect on increasing oil production. It is conducive to improving the rate of oil and natural gas extraction.[3] At present, the most commonly used proppant is the ceramic proppant prepared from bauxite. High-strength ceramic proppant prepared from high-grade bauxite is the mainstream material, widely used in industrial production.[4–5] However, bauxite belongs to non-renewable re-

*Corresponding author's e-mail:
yuruien@nuc.edu.cn (Ruien Yu)

© 2025 The Author(s). Except when otherwise noted, articles in this journal are published under the terms and conditions of the Creative Commons Attribution 4.0 International License (CC BY 4.0).

sources, and with the over-exploitation in recent years, its reserves have decreased, making the raw material cost of ceramic proppant increase significantly.[6] Ceramic proppant prepared from high-grade bauxite typically exhibits high bulk and apparent density, decreasing its ability to conduct fluid flow, therefore largely limiting its development and utilization in the field of oil and gas.[7]

In recent years, with the development of science and technology, as well as strengthening of people's environmental awareness and attention to the problem of solid waste,[8] many researchers have begun to pay great attention to the development of low-density and high-hardness ceramic proppant using low-grade bauxite ore or solid waste.[9–10] At the same time, it also helps solve the problems of environmental pollution caused by solid waste accumulation and improve the utilization rate of industrial waste.[11] Ren et al.[12] used solid wastes such as low-grade bauxite and fly ash as a novel route for preparing a high-silica proppant via sintering at 1240 °C for 20 min. The bulk density of the proppant was 1.352 g/cm^3, acid solubility was 4.2 %, and crushing rate was 5.3 %. Another experiment was conducted to find an effective and applicable method. Hao et al.[13] used low-grade bauxite, solid waste, coal gangue and magnesium slag to successfully prepare a low-cost ceramic proppant, sintered at 1250 °C, having a bulk density of not more than 1.5 g/cm^3, apparent density of less than 3.0 g/cm^3, closed pressure of 52 MPa, and the lowest crushing rate of 7.16 %. These raw materials greatly reduce the preparation cost of proppant, while the addition of solid waste not only relieves the environmental pressure, but also develops a new way of solid waste recycling. F. Kukurugya et al.[14] incorporated Cu-based oxygen carriers into high-strength ceramic fracturing proppant. The waste Cu-based oxygen carriers were successfully converted into high-strength ceramic spheres through three main steps: ball milling, granulation and sintering. The results show that the compressive strength can exceed 150 MPa at a sintering temperature of 1600 °C, while the $CuAl_2O_4$ phase melts and separates. The production of high-strength ceramic fracking proppant using waste Cu-based oxygen carriers not only reduces the problem of waste disposal, but also saves the scarce bauxite resources, leading to significant economic and environmental benefits.

At present, the world's aluminum ash production is huge, and it is mainly disposed in direct landfills or piles, which is not conducive to achieving resource utilization and sustainable development.[15] Secondary aluminum ash is the solid waste after the extraction of metallic aluminum from primary aluminum ash or aluminum-containing waste residue after aluminum extraction from aluminum slag. It is a hazardous solid waste containing a large number of toxic and harmful substances, such as aluminum nitride, aluminum carbide, fluoride, cyanide and others,[16] and its treatment has always been a research hotspot of the aluminum electrolysis industry.[17] Since secondary aluminum ash contains a large amount of alumina, its use as a raw material for the preparation of ceramic proppant not only reduces the problem of proppant preparation cost, but also promotes the reuse of secondary aluminum ash, thus alleviating the serious pollution of soil and water resources brought about by the large amount of secondary aluminum ash discharge.

In response to the above research, this paper studies the secondary aluminum ash and kaolin as raw materials, and manganese dioxide as an additive. It was found that an addition of manganese dioxide during sintering can well promote the high-temperature sintering performance, accelerate the rearrangement of mullite particles, and enhance the degree of densification of porous mullite.[18–20] A low-cost ceramic proppant was prepared by sintering to study the effect of manganese dioxide as an additive on the basic properties of secondary aluminum ash-based ceramic proppants (bulk density, apparent density, crushing rate). In addition, the effect of different levels of manganese dioxide on the phase composition and microstructure of the ceramic granule proppant was analyzed using XRD and SEM, in order to further explore the feasibility of utilizing low-cost hazardous solid waste.

2 EXPERIMENTAL PART

2.1 Preparation of ceramic support

The samples consisted of powdered secondary aluminum ash, whose purity was greater than 90 *w*/%, the particle size was 1–2 nm (Xinjiang Runlin Environmental Protection Co., Ltd.), and kaolin whose purity was greater than 24 *w*/% (Xinjiang Runlin Environmental Protection Co., Ltd.). The chemical compositions of the raw materials are shown in **Table 1**. Manganese dioxide acting as the additive was configured separately according to the proportions and mix configurations shown in **Table 2.** The mixed batch was first ball-milled in a planetary ball mill (XQM-2, Changsha Tianchuang Powder Technology Co., Ltd., China) at 400 min^{-1} for 10–15 min to mix the raw materials uniformly. Then, the homogeneously mixed raw materials were continuously added into a disc granulator, and the materials were continuously sprayed with water mist during rotation to generate raw-material ball blanks with increasing time. These ball blanks were sieved through a 20/40 mesh sieve. The sieved ball billets were put into corundum boats and dried in a drying oven (DHG-9055A, Shanghai Yiheng Scientific Instrument Co., Ltd., China) at about 80 °C for 4 h. The dried billets were put into a muffle furnace (MF-1200C, Anhui Beiyike Equipment Technology Co., Ltd., China) to be heated to 700 °C at 5 °C/min and kept hot for 1 h. After cooling, the billets were shaken and separated again. The preheated spherical billets were directly placed into a high-temperature atmosphere furnace (AS2-4-18TP, Zhengzhou Ansheng Scientific Instrument Co., Ltd., China) and heated at 5 °C/min to the predeter-

Table 1: Main chemical components of the raw materials

Material	Chemical composition, %								
	Al_2O_3	SiO_2	Na_2O	K_2O	CaO	TiO_2	Fe_2O_3	V_2O_5	MgO
Secondary aluminum ash	91.04	1.73	4.09	0.18	0.9	0.18	0.27	1.2	0
Kaolin	24.16	67.07	0	2.15	0.74	1.19	3.55	0	0.73

mined sintering temperature, followed by a holding time of 3 h. Afterwards, they were cooled to room temperature. The specimens were sieved through a 20–40 mesh sieve, and the testing was performed in strict accordance with the Chinese oil and gas industry standard SY/T5108-2014. **Figure 1** shows the appearance and morphology of the ceramic grains after the incorporation of the additive.

Table 2: Influence of MnO_2 on the properties of ceramic proppant

Manganese dioxide addition (*w*/%)	Sintering temperature (°C)	Bulk density (g/cm^3)	Apparent density (g/cm^3)	Crushing rate (%)
2	1230	1.1278	2.5646	15.84
	1250	1.2105	2.5073	9.64
	1270	1.2305	2.5033	8.41
4	1230	1.0998	2.4368	17.45
	1250	1.1409	2.4399	15.66
	1270	1.0813	2.4302	18.15
6	1170	1.0609	2.4219	18.85
	1190	1.0779	2.4192	17.65
	1210	1.0992	2.4007	17.17

2.2 Test and characterization

2.2.1 Bulk density test

A 50 mL density bottle was prepared and its mass (m_1) was measured using an electronic balance. The appropriate amount of ceramic grain samples was then weighed. A suitable funnel was secured above the mouth of the density bottle, then the proppant sample was poured through it until the bottle was filled to the graduated line. The mass of the density bottle containing the ceramic grain sample was measured (m_2). Bulk density was calculated using Equation (1), and the procedure was repeated several times to obtain an average value.

$$\rho_B = \frac{(m_2 - m_1)}{V} \quad (1)$$

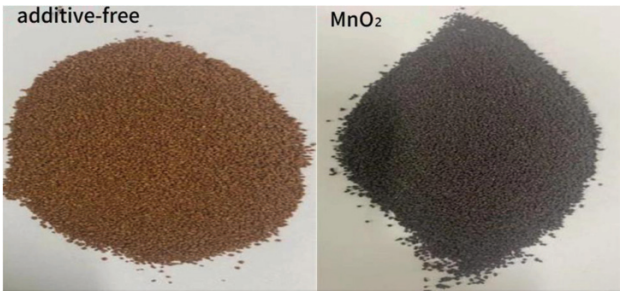

Figure 1: Effect of MnO_2 on the morphology of the ceramic support agent

Here, ρ is the proppant bulk density, g/cm^3; m_1 is the mass of density bottle, g; m_2 is the mass of proppant and density bottle, g; V is the volume of cylinder, mL.

2.2.2 Apparent density test

The ceramic sample mass (M) was weighed with an electronic balance; a 50 mL density bottle was cleaned and dried and its mass (m_1) was weighed with the electronic balance; the density bottle was filled with distilled water and its mass (m_2) was weighed with the electronic balance; distilled water from the density bottle was poured out and the weighed ceramic sample was poured into the density bottle, which was then refilled with distilled water; the mass (m_3) was weighed with the electronic balance; Equation (2) was calculated based on the density formula; the procedure was repeated several times to obtain an average value.

$$\rho_B = \frac{M}{\frac{(m_2 - m_1)}{\rho_w} - \frac{(m_3 - m_1 - M)}{\rho_w}} \quad (2)$$

Here, ρ is the apparent density of ceramic proppant, g/cm^3; M is the mass of ceramic sample, g; m_1 is the mass of density bottle, g; m_2 is the mass of density bottle filled with distilled water, g; m_3 is the mass of density bottle filled with distilled water and ceramic proppant, g; ρ_w is the apparent density of water, g/cm^3.

2.2.3 Crushing rate test

The main equipment used to test the crushing resistance of proppant samples was a YAW-300B type automatic compression and flexural testing machine, as shown in **Figure 2** illustrating the structure of the proppant crushing chamber. In accordance with Equation (3), the bulk density of the proppant sample was measured to determine the crushing rate of the sample; the required sample mass (m) was weighed and evenly spread into the crushing chamber; the piston was then inserted and rotated by 180°; the chamber was then placed at the center of the hydraulic machine table; the loading pressure of the hydraulic machine was set to 71 KN and the loading time was 1 min; this pressure was maintained for 2 min; after unloading, the proppant samples were taken out; after the hydraulic press crushing, the ceramic samples were collected and put onto a 40-mesh sieve for shaking; after sieving for 10 min, the mass (m_0) of the crushed proppant samples was weighed with the electronic balance; and the sample crushing rate was calculated in accordance with Equation (4).

$$m_p = C \cdot \rho \cdot d^2 \quad (3)$$

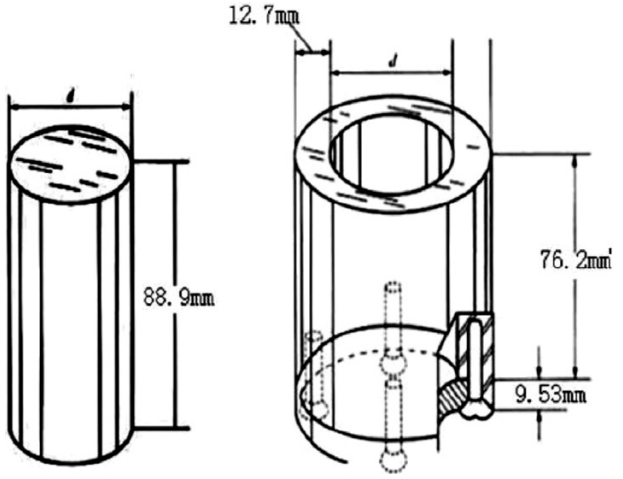

Figure 2: Structural diagram of proppant crushing chamber

Here, m_p is the total mass of proppant, g; ρ is the proppant bulk density, g/cm^3; d is the diameter of proppant crushing chamber structure, cm; C is the volume of proppant crushing chamber structure.

$$\eta = \frac{m_0}{m_p} \times 100\ \% \tag{4}$$

Here, η is the proppant fragmentation rate, %; m_p is the total mass of proppant before testing, g; m_0 is the mass of proppant particles after testing, g.

2.2.4 X-ray diffraction test

The X-ray test was carried out using a fully automatic polycrystalline X-ray diffractometer (XD-2/XD-3, Cu target, Beijing Puxi Analytical Instrument Co., Ltd.), Kα light source, λ = 0.154 nm, a scanning speed of 8 °/min, a scanning range of 10–90°, an operating voltage of 36 kV, and an operating current of 20 MA for the crystalline composition analysis of the samples.

2.2.5 Scanning electron microscope test

A Hitachi's SU3900 scanning electron microscope was used to observe and analyze the morphology of sample surfaces and the microstructure of samples, and then analyze the crystal growth condition and void development of the proppant samples.

3 RESULTS AND DISCUSSIONS

3.1 Effect of manganese dioxide on ceramic proppant

Figure 3 shows XRD patterns of the proppant samples at different sintering temperatures and manganese dioxide additions of (2, 4 and 6) *w*/%, and it was found that the main crystalline phase of the proppant samples was corundum.[21] When the manganese dioxide addition is 2 *w*/%, and the sintering temperature is increased from 1230 °C to 1270 °C, the corundum's diffraction peaks are gradually strengthened, becoming sharper, and the diffraction peak of mullite is weakened. As the manganese dioxide content increases to 4 *w*/% and the sintering temperature rises as well, the mullite phase of the sample gradually disappears, and the crystal phase of the sample includes corundum at 1270 °C. The analyses show that after increasing the amount of manganese dioxide, more liquid phase is formed in the sample under high-temperature sintering, dissolving the mullite phase. During the cooling of a sample, most of the liquid phase forms a glassy phase with a low strength, and this low-viscosity liquid phase fills in the voids during the cooling process, causing closed pores inside the proppant,[22] which greatly reduce the hardness of the proppant. When the manganese dioxide content is increased to 6 *w*/%, there are more impurities in the samples at lower sintering temperatures, with incompletely reacted manganese dioxide and manganese tetroxides, and a minor manganese-aluminum garnet crystalline phase. The analysis shows that the ionic radii of Mn^{4+} (0.053 nm) and Al^{3+} (0.0535 nm) are very close to each other, which makes the manganese dioxide and alumina undergo an infinite solid solution and form a solid solution. On the other hand, Mn^{4+} undergoes a reduction reaction during high-temperature sintering, which leads to a change in its ionic radius, altering the lattice of alumina and lowering the sample's sintering temperature, thus promoting sintering.

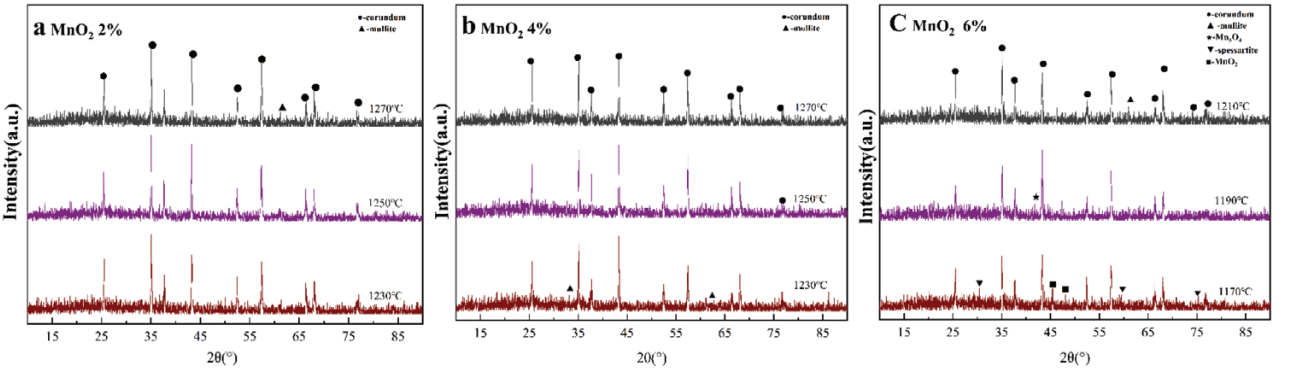

Figure 3: XRD diagrams of ceramic proppant with different manganese dioxide contents (a, 2 *w*/%; b, 4 *w*/%; c, 6 *w*/%) and different sintering temperatures

3.2 Effect of manganese dioxide on the microscopic morphology of ceramic proppant

Figure 4 shows the micromorphologies of the crushed sections of the proppant samples at different sintering temperatures and different manganese dioxide additions. **Figures 4a, 4b** and **4c** include SEM images of the manganese dioxide additions of 2 *w*/% at sintering temperatures of (1230, 1250 and 1270) °C, respectively. They show that the internal structure of a proppant sample is mainly covered with corundum on top of the liquid phase, and with the addition of manganese dioxide, the MnO_2-Al_2O_3-SiO_2 ternary eutectic system gradually increases, reducing the corundum generation temperature and increasing the corundum growth rate. It is shown that as the sintering temperature increases, the corundum keeps growing and the overall structure gradually becomes more compact. As a result, the bulk density of the proppant samples increases and the hardness is also increased.

Figures 4d, 4e and **4f** include SEM images of the manganese dioxide addition of 4 *w*/% at sintering temperatures of (1230, 1250 and 1270) °C, respectively. It can be seen that there are a few air holes inside the proppant samples, which may be due to the increase in the amount of manganese dioxide. At the higher temperatures MnO_2 is more sensitive to decomposition and oxygen production. MnO_2 undergoes the first two steps of the reaction, first transforming into Mn_2O_3 ($4MnO_2 \rightarrow 2Mn_2O_3 + O_2$) and then, with the increase in the temperature, Mn_2O_3 further transforms into Mn_3O_4, ($6Mn_2O_3 \rightarrow 4\ Mn_3O_4 + O_2$) while releasing oxygen. This gas release causes closed pores to form inside the ceramic samples. The formation of these pores not only reduces the density of the samples (as evidenced by a decrease in the apparent density), but also significantly weakens its compressive strength. From **Figures 4e** and **4f**, it can be seen that with increasing sintering temperature, the densification is not as high as in the proppant samples with 2 *w*/% manganese dioxide addition.

Figures 4g, 4h and **4i** include SEM images of the samples at sintering temperatures of (1170, 1190 and 1210) °C, respectively, with 6 *w*/% manganese dioxide addition. We can see that a large number of air holes appear in the internal part of a proppant sample, which is due to the excessive content of manganese dioxide, resulting in a continuous gas generation, reducing the density of the proppant sample, but also leading to decreased hardness. Additionally, we found that when the MnO_2 content is 6 *w*/%, the increased liquid phase volume leads to an excessive grain growth and the formation of large-grain boundary pores, further enhancing the deterioration in mechanical properties. When the MnO_2 addition is 2 *w*/%, liquid-phase sintering promotes pore closure, forming a dense structure. However, excessive MnO_2 introduces interconnected pores through decomposition reactions and liquid-phase contraction, acting as stress concentration points and leading to a decrease in strength.

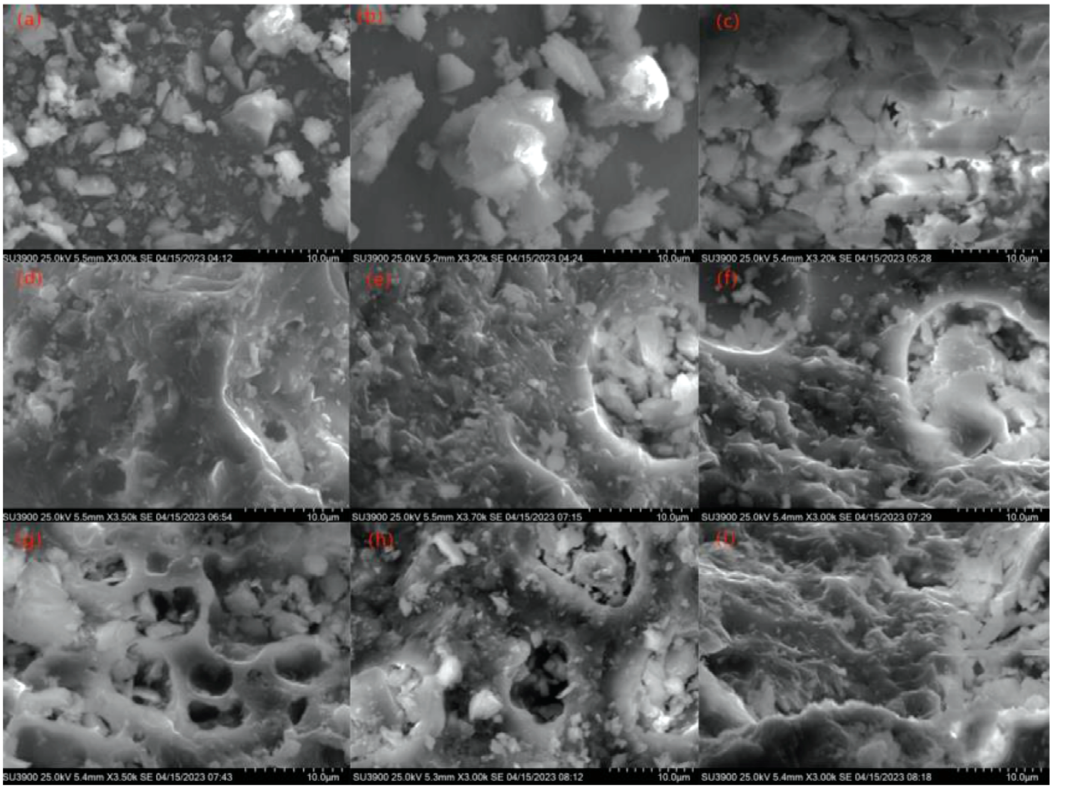

Figure 4: SEM images of ceramic proppant with different manganese dioxide contents at different sintering temperatures

3.3 Effect of manganese dioxide on apparent density and bulk density of ceramic proppant

Figure 5 shows the changing curves of the apparent density and bulk density of the proppant samples with the increase in the sintering temperature at different manganese dioxide additions. **Figure 5a** shows that when manganese dioxide amount is 2 *w*/%, the apparent density of the proppant samples generally shows a decreasing trend and the bulk density shows an increasing trend in a range of 1230–1270 °C. Due to the addition of manganese dioxide, the influence of the fluxing effect becomes larger; the liquid phase in the ternary eutectic system becomes more significant with the increase in the temperature; the densification of the sample is gradually enhanced, increasing the bulk density; and the liquid phase enters the stomatal pores under the effect of surface tension, constantly filling the voids, which makes the porosity decrease and the apparent density decrease.

Figure 5b shows that the apparent density of the proppant samples gradually decreases and the bulk density first increases and then decreases in the range of 1230–1270 °C with the 4 *w*/% manganese dioxide addition.[23] As the amount of manganese dioxide increases, more liquid phase is formed under high temperature sintering, and the bulk density of the samples gradually increases under the temperatures of 1230 °C and 1250 °C. When the sintering temperature continues to increase to 1270 °C, recrystallisation occurs through the action of the liquid phase, during which the condensed liquid phase promotes crystal growth. In addition, the inter-granular voids gradually increase, thus affecting the densification of the proppant samples, resulting in a decrease in bulk density. **Figure 5c** represents the sample with a manganese dioxide additive amount of 6 *w*/%. The apparent density shows a downward trend, while the bulk density shows an upward trend. Experimental analysis showed that with the increase in the manganese dioxide content, the liquid phase in the MnO_2-Al_2O_3-SiO_2 ternary eutectic system increases, and its fluxing effect is greatly improved.

3.4 Effect of manganese dioxide on the crushing rate of ceramic proppant

Figure 6 shows variations in the crushing rate of the proppant samples with increasing sintering temperature and different manganese dioxide additions. **Figure 6a** shows that the crushing rate of the proppant sample with the addition amount of 2 *w*/% gradually decreases in a range of 1230–1270 °C, while it is only 8.41 % at 1270 °C, under sealed conditions at 35 MPa. Due to the addition of manganese dioxide, a low-temperature eutectic can readily form, which promotes the generation of a liquid phase and improves densification. At the same time, the corundum generation temperature is reduced to a certain extent and the growth rate of corundum is increased, thus improving the strength of the proppant sample. **Figure 6b** shows that with the addition amount of 4 *w*/% and increasing sintering temperature, the crush-

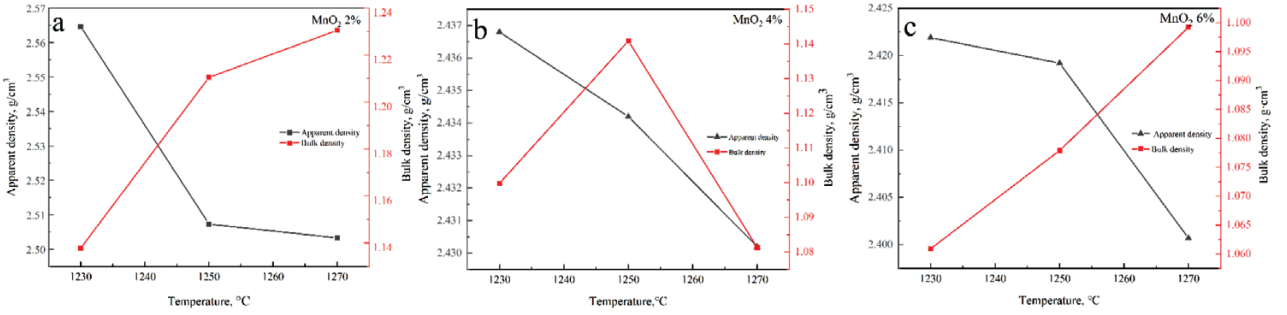

Figure 5: Bulk density and apparent density of ceramic proppant with different manganese dioxide contents (a, 2 *w*/%; b, 4 *w*/%; c, 6 *w*/%) at different sintering temperatures

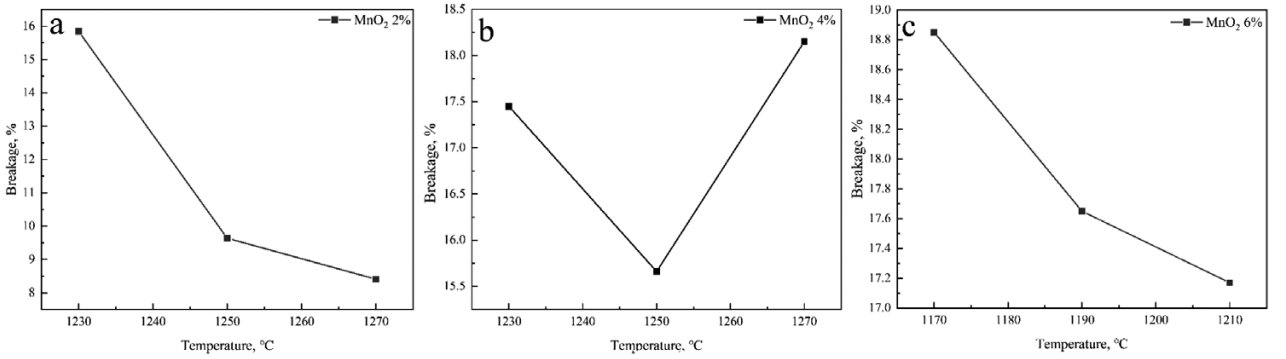

Figure 6: Breakage rate of ceramic proppant with different manganese dioxide contents: a) 2 *w*/%; b) 4 *w*/%; c) 6 *w*/%) at different sintering temperatures

ing rate of the proppant sample first decreases and then increases. Based on SEM analysis and bulk density changes, it can be seen that with the increase in the manganese dioxide content, decomposition occurs at high temperatures, generating more gases inside, thereby increasing internal porosity. Moreover, with the increase in the temperature, numerous liquid phases form within the samples. Upon cooling, these transform into a glassy phase, resulting in an increased fragmentation rate at 1270 °C. **Figure 6c** shows that at the addition of 6 wt.%, the sintering temperature of the sample is greatly reduced due to the large content of manganese dioxide, which promotes the generation of a liquid phase. As can be seen from the figure, the crushing rate of the proppant samples gradually decreases in a sintering-temperature range of 1170–1210 °C.

4 CONCLUSIONS

In this paper, a low-cost and high-strength secondary aluminum ash-based ceramic proppant was successfully prepared using secondary aluminum ash as the main raw material, kaolin as the auxiliary material and manganese dioxide as the additive. At a sintering temperature of 1270 °C, and a manganese dioxide amount of 2 *w*/%, the ceramic proppant exhibits the best performance. Its main crystalline phase is corundum, accompanied by a small amount of mullite, with a bulk density of 1.2305 g/cm^3, an apparent density of 2.5033 g/cm^3, and a crushing rate of 8.41 % under sealed conditions at 35 MPa, satisfying the industry standard. With the addition of manganese dioxide, the ternary eutectic system of MnO_2-Al_2O_3-SiO_2 gradually increases, reducing the corundum generation temperature and accelerating the growth of corundum. The liquid phase in the ternary eutectic system increases with increasing temperature, which leads to the densification of the proppant sample. The liquid phase enters the pores and fills the voids under surface tension, resulting in a decrease in apparent porosity and an increase in closed porosity, further leading to a decrease in apparent density. As the sintering temperature increases, corundum grows continuously, and the overall structure gradually becomes compact. The bulk density increases, and the hardness is enhanced. At this point, the number of mullite phases is relatively small and the number of corundum phases is large. Through experimental research, the breakage rate of the 2 *w*/% MnO_2 sample decreased to 8.41 % at 1270 °C, meeting the lower limit requirement from the SY/T 5108-2014 standard. However, it still falls short of the performance standards for high-performance proppants. This study found, for the first time, that the compressive strength of secondary aluminum ash-based proppants has been improved to an industry-acceptable level, although it remains at the lower limit, leaving room for further optimization.

Acknowledgements

This work was supported by the Opening Project of Xinjiang Key Laboratory of High Value Green Utilization of Low-Rank Coal [Grant No. XJDX2314-YB202403] and the Teaching Reform of Education in Xinjiang Uygur Autonomous Region [XJGXPTJG-202262, XJ2024GY32].

5 REFERENCES

[1] J. M. Fan, T. P. Bailey, Z. Q. Sun, P. C. Zhao, C. Uher, F. L. Yuan, M. Y. Zhao, Preparation and properties of ultra-low density proppants for use in hydraulic fracturing, Journal of Petroleum Science and Engineering, 163 (**2018**), 100–109, doi:10.1016/j.petrol.2017.10.024

[2] Y. C. Feng, C. Y. Ma, J. G. Deng, X. R. Li, M. M. Chu, H. Cheng, Y. Y. Luo, A comprehensive review of ultralow-weight proppant technology, Petroleum Science, 18 (**2021**), 807–826, doi:10.1007/s12182-021-00559-w

[3] K. Razminia, A. Razminia, D. F. M. Torres, Pressure responses of a vertically hydraulic fractured well in a reservoir with fractal structure, Applied Mathematics and Computation, 257 (**2015**), 374–380, doi:10.1016/j.amc.2014.12.124

[4] X. L. Wu, Z. Z. Huo, Q. Ren, H. H. Li, F. Lin, T. Y. Wei, Preparation and characterization of ceramic proppants with low density and high strength using fly ash, Journal of Alloys and Compounds, 702 (**2017**), 442–448, doi:10.1016/j.jallcom.2017.01.262

[5] X. D. Chen, T. H. Li, T. H. Zhao, H. Li, A. L. Dang, Y. D. Shang, Y. Zhang, Effect of MnO_2 on the Properties of Mullite-Based Ceramics, Chemistry Letters, 46 (**2017**), 327–329, doi:10.1246/cl.161012

[6] X. Zhao, W. X. Li, X. R. Zhang, Y. F. Xue, J. B. Mu, D. F. Xu, W. P. Li, Y. M. Wang, S. J. Qin, Z. X. Zhang, Low-temperature preparation of lightweight ceramic proppants using high-proportioned coal-based solid wastes, Ceramics International, 50 (**2024**) 11, 18117-18124, doi:10.1016/j.ceramint.2024.02.295

[7] D. H. Ding, Y. F. Fang, G. Q. Xiao, X. F. Zhu, P. C. Fu, X. C. Chong, Effects of sintering temperature on microstructure and properties of low-grade bauxite-based ceramic proppant, International Journal of Applied Ceramic Technology, 18 (**2021**) 5, 1832–1844, doi:10.1111/ijac

[8] S. Y. Wang, B. Liu, Q. Zhang, Q. Wen, X. H. Lu, K. Xiao, C. Ekberg, S. G. Zhang, Application of geopolymers for treatment of industrial solid waste containing heavy metals: State-of-the-art review, Journal of Cleaner Production, 390 (**2023**), 136053, doi:10.1016/j.jclepro.2023.136053

[9] J. Z. Zhao, Z. L. Liu, Y. M. Li, Preparation and characterization of low-density mullite-based ceramic proppant by a dynamic sintering method, Materials Letters, 152 (**2015**), 72–75, doi:10.1016/j.matlet.2015.03.060

[10] X. X. Ma, Y. M. Tian, Y. Zhou, K. Y. Wang, Y. S. Chai, Z. G. Li, Sintering temperature dependence of low-cost, low-density ceramic proppant with high breakage resistance, Materials Letters, 180 (**2016**), 127–129, doi:10.1016/j.matlet.2016.04.080

[11] Y. Q. Shao, W. Y. Zhang, Y. Zhu, T. Dou, L. Z. Chu, Z. D. Liu, Preparation of municipal solid waste incineration fly ash-based ceramsite and its mechanisms of heavy metal immobilization, Waste Management, 143 (**2022**), 54–60, doi:10.1016/j.wasman.2022.02.021

[12] Q. Ren, Y. H. Ren, H. H. Li, X. L. Wu, W. N. Bai, J. L. Zheng, O. Hai, Preparation and characterization of high silicon ceramic proppants using low grade bauxite and fly ash, Materials Chemistry and Physics, 230 (**2019**), 355–361, doi:10.1016/j.matchemphys.2019.04.009

[13] J. Y. Hao, H. Q. Ma, X. Feng, Y. F. Gao, K. Y. Wang, Y. M. Tian, Low-temperature sintering of ceramic proppants by adding solid wastes, International Journal of Applied Ceramic Technology, 15 (**2018**) 2, 563–568, doi:10.1111/ijac.12818

[14] F. Kukurugya, J. Bergmans, R. Snellings, J. Spooren, Recycling of spent Cu-based oxygen carriers into high-strength ceramic proppants, Ceramics International, 43 (**2017**) 18, 16895–16902, doi:10.1016/j.ceramint.2017.09.090

[15] M. Mahinroosta, A. Allahverdi, Hazardous aluminum dross characterization and recycling strategies: A critical review, Journal of Environmental Management, 223 (**2018**), 452–468, doi:10.1016/j.jenvman.2018.06.068

[16] Y. H. Wang, Y. Lan, Y. H. Hu, Adsorption mechanisms of Cr (VI) on the modified bauxite tailings, Minerals Engineering, 21 (**2008**) 12–14, 913–917, doi:10.1016/j.mineng.2008.04.003

[17] Y. Shi, K. X. Jiang, T. A. Zhang, Cleaner extraction of alumina from coal fly ash: Baking-electrolysis method, Fuel, 273 (**2020**), 117697, doi:10.1016/j.fuel.2020.117697

[18] W. W. Yang, Y. F. Zhang, Effects of MnO_2 addition on the microstructure and dielectric properties of $LiTaO_3$ ceramics, 173 (**2020**), 109130, doi:10.1016/j.vacuum.2019.109130

[19] A. N. Chen, L. Lu, L. J. Cheng, J. M. Wu, R. Z. Liu, S. Chen, Y. Chen, S. F. Wen, C. H. Li, Y. S. Shi, TEM analysis and mechanical strengthening mechanism of MnO_2 sintering aid in selective laser sintered porous mullites, Journal of Alloys and Compounds, 809 (**2019**), 151809, doi:10.1016/j.jallcom.2019.151809

[20] C. W. Nahm, Effect of MnO_2 addition on microstructure and electrical properties of $ZnO–V_2O_5$-based varistor ceramics, Ceramics International, 35 (**2009**) 2, 541–546, doi:10.1016/j.ceramint.2008.01.010

[21] Y. M. Tian, P. F. Zhao, X. C. Kong, The Effect of Sintering Temperature on the Structure and Properties of Corundum/Mullite Ceramics, Science of Sintering, 47 (**2015**) 3, 273–278, doi:10.2298/SOS1503273Y

[22] V. V. Pogrebenkova, T. V Vakalova, V. V. Gorbatenko, M. V. Grekhova, Features of phase formation of mullite-corundum materials in mixtures of kaolin with a fluoriding component, Advances in Applied Ceramic, 51 (**2010**), 197–201, doi:10.1007/s11148-010-9288-3

[23] X. C. Kong, Y. M. Tian, Y. S. Chai, P. F. Zhao, K. Y. Wang, Z. G. Li, Effects of pyrolusite additive on the microstructure and mechanical strength of corundum-mullite ceramics, Ceramics International, 41 (**2015**) 3, 4294–4300, doi:10.1016/j.ceramint.2014.11.116